tered with AII (100 ng/min; Peptide Institute Inc., Osaka, Japan) using Alzet osmotic pumps (DURECT Co., Cupertino, Calif., USA) (A group, n = 11). In the fourth group, rats were administered with both HV and AII (H+A group, n = 22). Rats were sacrificed on day 1, 2, 3 or 4, and kidneys excised for histochemical analysis (fig. 1).

Measurement of Systolic Blood Pressure

Systolic blood pressure (SBP) was measured by the tail-cuff method with an electro-sphygmomanometer (BP-98A; Softron Co., Tokyo, Japan). SBP was measured in conscious rats every day from day 1 to 2. The SBP value for each rat was calculated as the average of 3 separate measurements at each session. SBP measurement was performed between 9 and 12 a.m. by a single blinded investigator.

Measurements of Serum Urea Nitrogen and Creatinine

Before the sacrifice, blood samples were obtained via an axillary vein for determination of serum urea nitrogen (UN) and creatinine (Cr) levels. Serum UN and Cr levels were determined enzymatically with automation-analysis equipment (Hitachi 7350; Hitachi Co., Ibaragi, Japan) in our laboratory center.

Histological Analysis

To evaluate the progression of GN in our animal model, histological analyses were performed using the periodic acid-Schiff (PAS) and periodic acid-methenamine silver (PAM) reagents. After the specimens were paraffin embedded, 4-μm-sectioned samples were stained with PAS and PAM reagents and counterstained with hematoxylin. For quantitative analysis, the ratio of damaged glomeruli to all glomeruli in the sectioned sample was calculated and the percentage of GN in the section was evaluated. Moreover, semiquantitative analysis was performed to evaluate more precisely the morphological changes of our GN model according to the protocol in previous studies [16, 17]. A minimum of 20 glomeruli (ranging from 20 to 60 glomeruli) in each specimen were examined and the severity of the mesangiolysis lesion was graded from 0 to 4+ according to the percentage of glomerular involvement; a 1+ lesion represented an involvement of 25% of the glomerulus while a 4+ lesion indicated that 100% of the glomerulus was involved. Thus, the mesangiolysis score (MES) was then obtained by multiplying the degree of damage (0 to 4+) by the percentage of the glomeruli with the lesion. Tubular injuries including tubular necrosis or occlusion of collecting ducts by cast material were graded as mild (1+), moderate (2+), or severe (3+).

Western Blot Analysis

Nuclear protein from whole kidney was prepared using NE-PER Nuclear and Cytoplasmic Extraction Reagents (Pierce Biotechnology Inc., Rockford, Ill., USA). Nuclear protein was electrophoresed using 10% SDS-PAGE gels and transferred to polyvinylidene difluoride membrane (Immobilon-P; Millipore Corp., Bedford, Mass., USA). A monoclonal IgG HIF-1α antibody α67 (Novus Biological, Littleton, Colo., USA) was used; a horseradish peroxidase-conjugated antibody (Promega Co., Madison, Wisc., USA) was used as a secondary antibody. The ECL Western blotting systems (Amersham Bioscience, Uppsala, Sweden) was used for detection.

Immunohistochemical Analysis

Paraffin sections including the samples were dewaxed in xylene and rehydrated in a series of ethanol, and then washed in distilled water before staining procedures. According to the instruction provided by the manufacturer, HIF-1α was identified with rabbit polyclonal anti-HIF-1α antibody H-206 (Santa Cruz Biotechnology, Calif., USA) utilizing the catalyzed signal amplification system (Dako, Hamburg, Germany) based on the streptavidin-biotin-peroxidase reaction. Antigen retrieval was performed for 5 min in a preheated Dako target retrieval solution using a microwave. Incubation procedures were performed in a humidified chamber. Following the incubation, specimens were washed 3 times in TBST buffer. The specificity of staining was confirmed by substitution of the primary antibody for a normal rabbit IgG and additionally by an immunohistochemical reaction without a primary antibody but with the secondary antibody alone.

An Experiment Using Cobalt Chloride as a Pretreatment

Rats were twice subcutaneously administered 30 mg/kg of cobalt chloride ($CoCl_2$) at a 12-hour interval ($CoCl_2$ group) (n = 11), followed by unilateral nephrectomy. Then, the rats were administered with HV and AII. As a comparison, rats were injected with 0.9% NaCl solution instead of $CoCl_2$, followed by the same protocol as the $CoCl_2$ group (n = 11). After $CoCl_2$ administration, however, before injection of HV and AII, a kidney was excised as a sample to examine expression level of HIF-1α ($CoCl_2$ Pre). Likewise, 2 days after administration of HV and AII, a kidney was also excised ($CoCl_2$ Day 2). To compare the expression level of HIF-1α by $CoCl_2$ before GN and the severity of pathology of GN, we investigated whether preinduction of HIF-1α is involved in renal protection.

Statistical Analysis

Data are reported as mean ± SEM. A paired t test was used for paired samples and Student's t test was used to compare the 2 groups. One-way layout analysis of variance or repeated measures of analysis of variance were used to compare multiple groups. If the p value was significant, Scheffé's multiple comparison was performed. A p value <0.05 was considered significant.

Results

AII Combined with HV Developed GN

Morphological studies using PAS and PAM staining revealed that there are no glomerular or tubular injuries in N group (fig. 2a), HV group (fig. 2b), A group (fig. 2c), however, GN was detected only in the H+A group (fig. 2e). Although renal tubular casts were observed, glomerular changes were scarcely observed on day 1 after AII and HV administration (fig. 2d, 3). GN was initially detected on day 2 (fig. 2e, f, 3), followed by further aggravation during the time course (data not shown). Renal tubular injury including tubular necrosis was not remarkable, and extensive cellular infiltration was not found in the interstitial regions (fig. 3). On the other hand, characteristic focal and segmental mesangiolysis, explained as capillary aneurysmal ballooning, was observed with dilatation of glomerulus (fig. 2e, f). The rate of occurrence of GN on day 2 was 44.9 ± 2.6%, and the MES score of the H+A

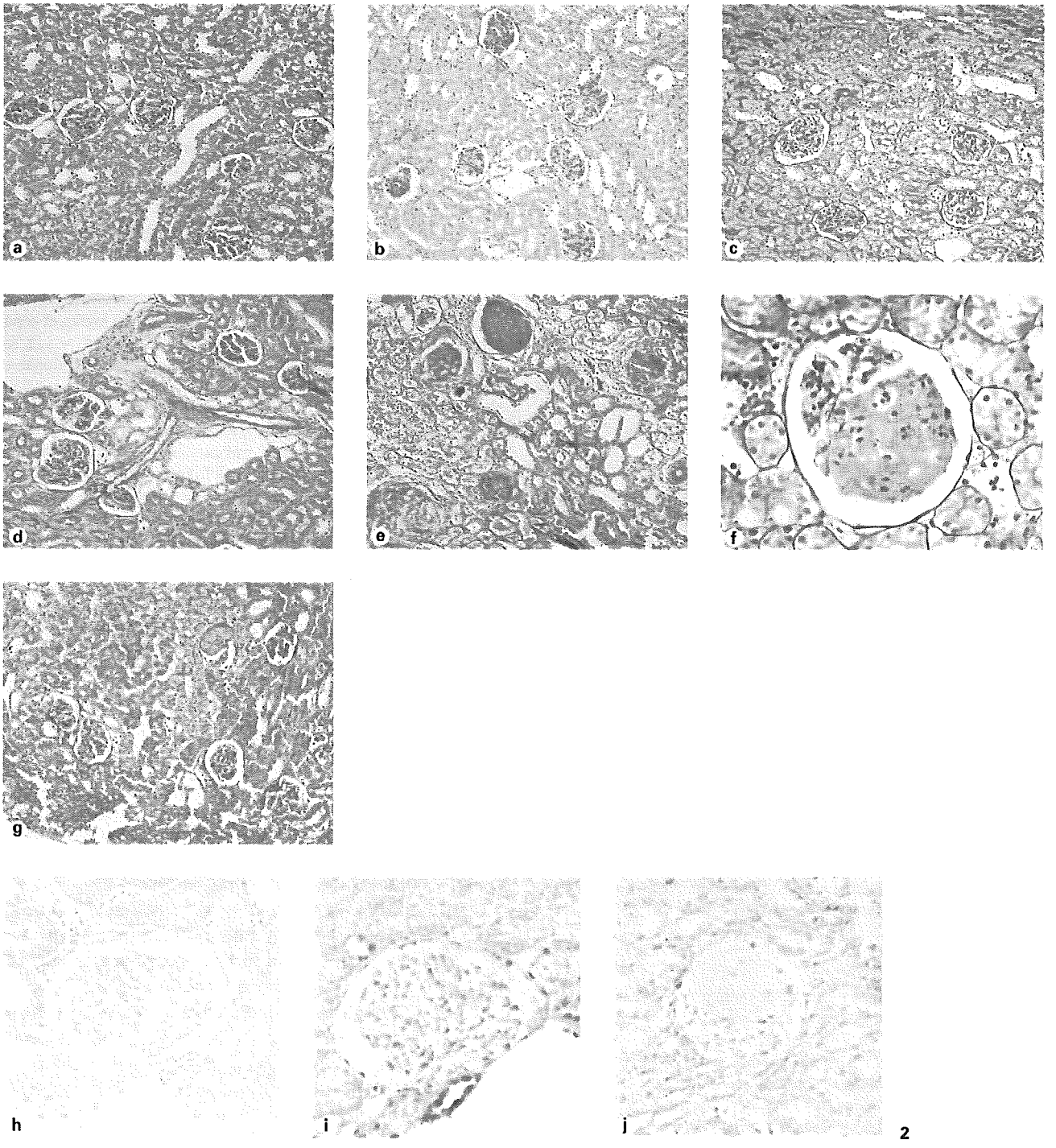

2

group was 199 ± 15 (fig. 3). On the other hand, in the HV group, less than 2% had morphologic changes of mesangiolysis during 4 days, and the MES score was 10 ± 5 (fig. 2b, 3). Moreover, in the A group, there were no morphologic changes during the time course (fig. 2c).

Changes in Serum UN and Cr

Serum UN and Cr were 18.4 ± 0.7 and 0.31 ± 0.01 mg/dl, respectively, on day 2 in the N group. In the H+A group, serum UN and Cr levels increased to 41.5 ± 4.0 and 0.57 ± 0.05 mg/dl, respectively, on day 2; significantly higher than those in the N group (fig. 4a, b). In contrast, serum UN and Cr levels in the H+A group on day 1 (24.0 ± 1.8 and 0.42 ± 0.02 mg/dl, respectively) were similar to the level of the N group. There were no significant differences in serum UN and Cr level among the HV, A and N groups.

SBP Response

SBP values of each group are shown in figure 4c. There were no significant differences in SBP after nephrectomy among the 4 groups. Administration of AII caused a significant increase of SBP on day 1 (186 ± 4 mm Hg) and persisted to day 2 (192 ± 1 mm Hg). SBP in the H+A group on day 2 (183 ± 3 mm Hg) was comparable to that in the A group. Administration of HV had no influence on SBP during the 2 days.

Expression Level of HIF-1α Protein

Western blot analysis revealed that the expression level of HIF-1α protein increased in the H+A and A groups (fig. 5a), compatible with the results of immunohistochemical analysis. Expressions of HIF-1α protein were observed in the A and H+A groups, but protein expression was not detected in the N and HV groups. These data suggest that HIF-1α was induced mainly by AII, and, at least in part, was related to the pathogenesis of GN or to the defense mechanism against the progression of GN.

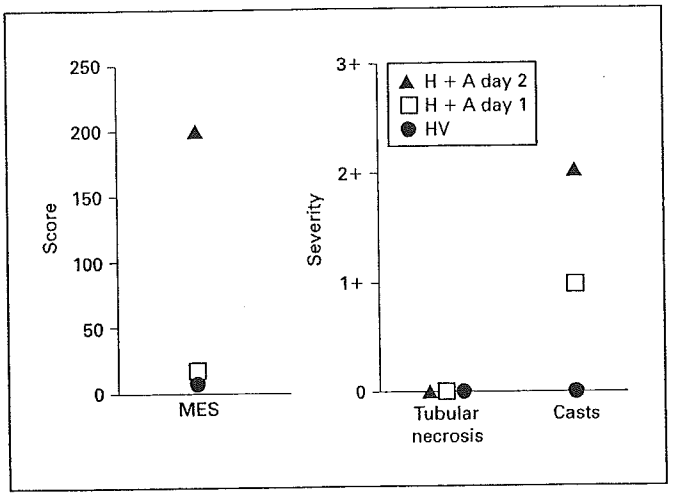

Fig. 3. Semiquantitative analysis of morphologic changes in our glomerulonephritis model. The main lesion in the H+A group is initially detected on day 2 as mesangiolysis in glomeruli; however, there are no tubular lesions of necrosis except for tubular casts; in contrast, there are no morphological changes in the N and A groups. MES = Mesangiolysis score.

Induction of HIF-1α in Glomeruli and Renal Tubules

Immunohistochemical study demonstrated positive nuclear staining of HIF-1α in glomeruli, renal tubules (fig. 2i, j), collecting ducts and epithelium of the papilla (data not shown) in the A and H+A groups. In contrast, no positive nuclear signals were detected in the N (fig. 2h) and HV (data not shown) groups. HIF-1α-positive cells were mainly detected in mesangial cells in glomeruli (fig. 2i, j). As demonstrated, especially in the H+A group (fig. 2j), HIF-1α was expressed in the intact part of the glomerulus, but not in the injured part of the same glomerulus. Furthermore, nuclear HIF-1α-positive signals were observed in smooth muscle cells in peripheral renal arteries (data not shown).

$CoCl_2$ Pretreatment Inhibits the Progression of GN

To further investigate whether HIF-1α is involved in the development of nephropathy or in the antiprogressive action, we pretreated rats with $CoCl_2$. As demonstrated in figure 5b, pretreatment with $CoCl_2$ increased HIF-1α expression before administration of HV and AII (Pre-1),

Fig. 2. Glomerulonephritis is developed with the combination of HV and AII, and HIF-1α is induced in the intact glomeruli. There are no glomerular or tubular injuries in N group (**a**), HV group (**b**), A group (**c**) and H+A group on day 1 (**d**). Damaged glomeruli, characterized by extensive mesangiolysis, are observed in H+A group on day 2. PAS staining. Magnification, ×100 (**e**). Focal and segmental mesangiolysis with large capillary aneurysmal ballooning are observed in the H+A group on day 2. PAM staining. Magnification, ×400 (**f**). The number of GN was significantly less in pretreatment with $CoCl_2$ than without. PAS staining. Magnification, ×100 (**g**). Immunoreactive HIF-1α-positive signals are not detected in the N group (**h**). Nuclear HIF-1α signals are observed in a glomerulus and tubules in the A group. Magnification, ×200 (**i**). A glomerulus in the H+A group on day 2 possesses intact cells with HIF-1α-positive signals; in contrast, other parts have few HIF-1α signals due to mesangiolysis. Magnification, ×200 (**j**).

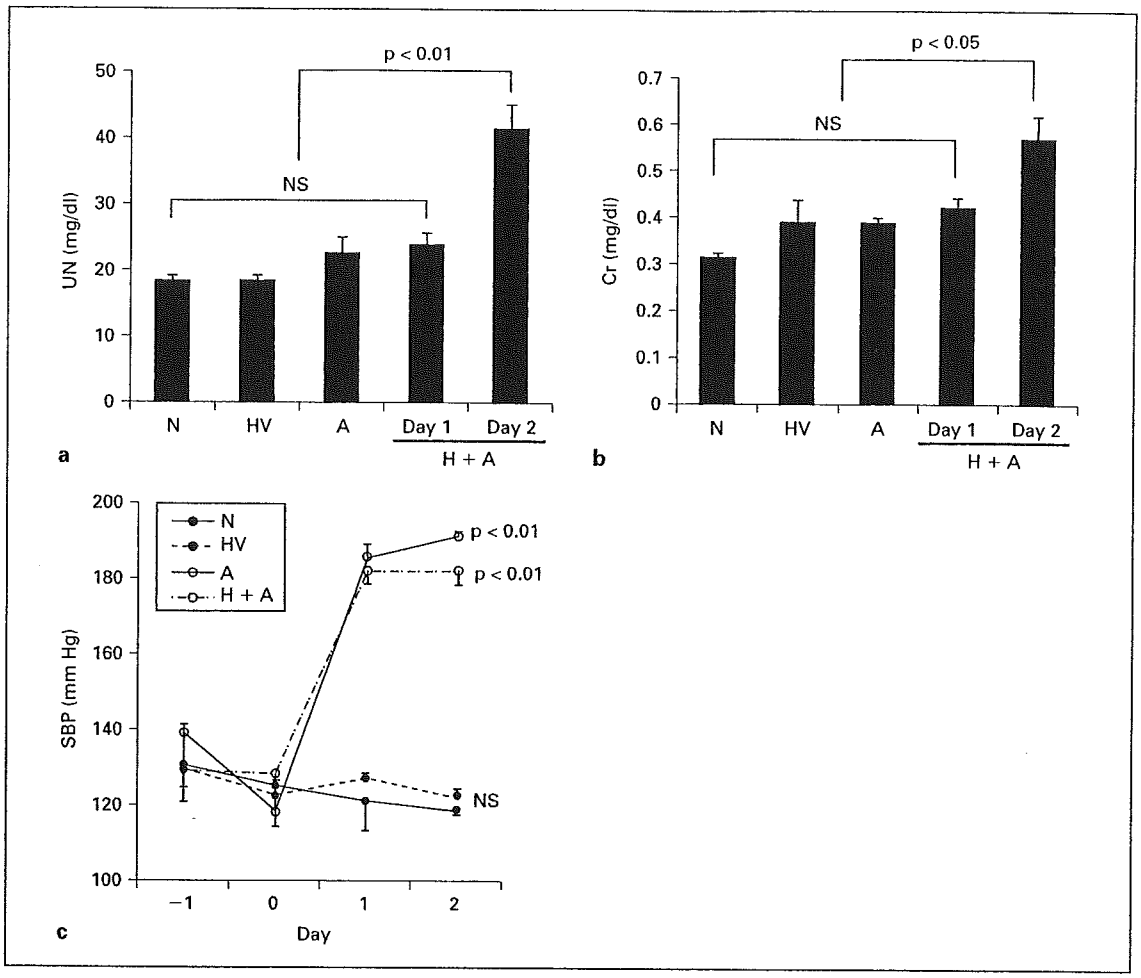

Fig. 4. Serum UN, Cr and SBP are increased with the combination of HV and AII. The serum UN (**a**) and Cr (**b**) levels in the H+A group on day 2 are significantly higher than other groups. SBP increases significantly with administration of AII (A and H+A groups) (**c**).

suggesting that HIF-1α was induced by $CoCl_2$ before development of GN. Even on day 2, the expression level of HIF-1α was increased in the $CoCl_2$ group ($CoCl_2$ Day 2-1). In the $CoCl_2$ group, focal mesangiolysis with glomeruli enlargement was still observed, but the number of GN was much less than in those without $CoCl_2$ pretreatment (fig. 2g).

Thus, 7 of 11 rats (63.6%) with $CoCl_2$ pretreatment were rescued from GN alone, while the other 4 (36.4%) were not; showing a comparable severity level of GN with the non-$CoCl_2$ group. As demonstrated in figure 5b, unlike Pre-1, Pre-2 did not induce HIF-1α with $CoCl_2$ and showed no $CoCl_2$ suppression of GN. The ratio between rats rescued or not rescued from GN was comparable with that between preinduction and noninduction of HIF-1α by $CoCl_2$, as demonstrated in figure 5c. In the $CoCl_2$ group, the rate of GN from each rat decreased to 12.2 ± 2.1%, which was in great contrast to 44.9 ± 2.6% in the non-$CoCl_2$ group. Furthermore, serum UN and Cr levels on day 2 were significantly lower in the $CoCl_2$ than in the non-$CoCl_2$ group ($p < 0.05$) (fig. 6a, b), despite comparable SBP values between the 2 groups (fig. 6c).

Discussion

In this study, we developed a new model of GN induced by both HV and AII. This model has several distinct characteristics. First, GN developed rapidly, and was detected on the second day after administration of

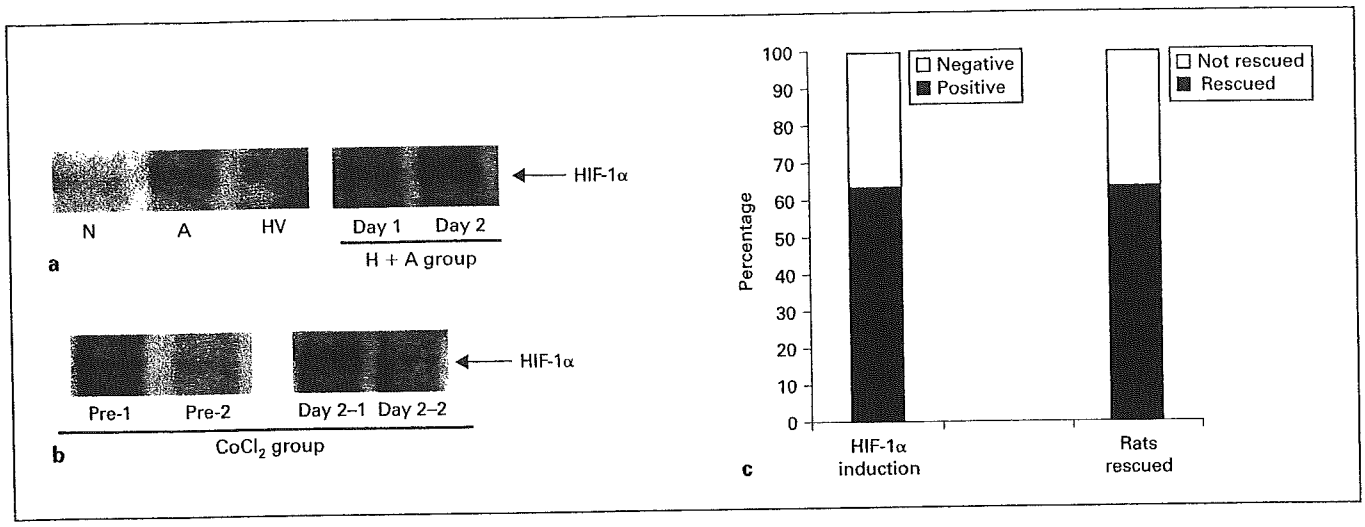

5

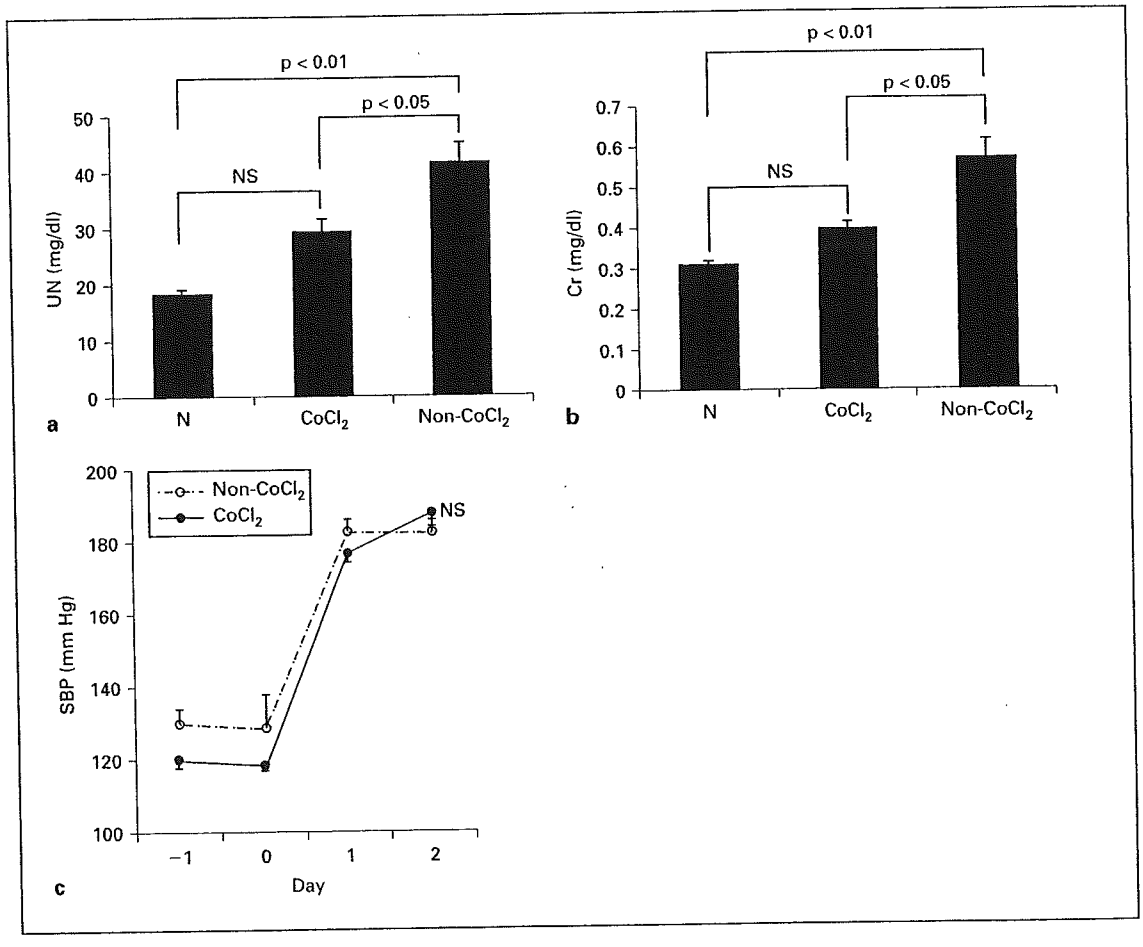

6

Fig. 5. The protein level of HIF-1α is increased by administration of HV and AII, and pretreatment of $CoCl_2$ increases HIF-1α expression before development of GN. HIF-1α is not detected in the N and HV groups (Day 2). However, HIF-1α is detected in A (Day 2) and H+A (Days 1 and 2) groups (**a**). The $CoCl_2$ group, in accord with the level of HIF-1α induction, was divided into 2 groups. HIF-1α is greatly induced before the development of GN ($CoCl_2$ group Pre-1), and is followed by a high level ($CoCl_2$ group Day 2-1); in contrast, it is not efficiently induced ($CoCl_2$ group Pre-2), and also is scarcely detected on day 2 ($CoCl_2$ group Day 2-2) (**b**). The rate of preinduction of HIF-1α by $CoCl_2$ is comparable with that of the inhibition of GN by $CoCl_2$ (**c**).

Fig. 6. Pretreatment with $CoCl_2$ attenuates GN. Serum UN (**a**) and Cr (**b**) levels in the $CoCl_2$ group on day 2 are significantly decreased compared to those in the non-$CoCl_2$ group. There is no significant difference in SBP between the $CoCl_2$ and non-$CoCl_2$ groups (**c**).

HV and AII. Many models of GN have been reported including 5/6 nephrectomized and Thy-1.1 nephritis models [18, 19]. However, these models take a long time to develop nephropathy. In contrast, our protocol induced GN in 2 days, suggesting that one of the advantages our model has over others is in terms of the time course. Further, pathological findings were restricted to glomerular regions without remarkable tubular or interstitial lesions. Since our GN model developed within 2 days, it also has advantages for disclosing the specifically critical time point of the development of GN. Furthermore, the development rate of GN was almost 100%, indicating the high reproducibility of our model. This basis of the rat model was initially developed by Barnes et al. [20] who reported that the progression of AII-induced renal injury was accelerated by pre-existing injury induced by HV; our model, which now optimizes the reproducibility of GN, is a modification of theirs.

Habu-induced nephropathy was reported to develop within 1 day by a dose of 2.0–4.0 mg/kg HV (in our model 3.5 mg/kg) and the main pathological change was 'mesangiolysis' [21, 22]. However, for reasons we have not as yet ascertained, in our study no rats showed Habu-nephropathy-specific pathological findings during the first week in the HV group. On the other hand, AII is one of the major factors responsible for the pathogenesis of GN, because it remarkably increases glomerular pressure causing hyperfiltration, production of extracellular matrix and expression of lines of genes involving GN [23–25]. Further, since AII has some ischemic effects on the kidneys, there is the possibility that an AII-induced ischemic effect causes the GN depicted in our model. However, as demonstrated in this study, glomerular injury was predominantly observed, and was not associated with renal tubular lesions, i.e. tubular necrosis suggesting renal ischemia. Therefore, in accordance with the pathological characteristic of this GN, AII-induced renal ischemia may not be responsible for its development in our model. Additionally, in this study, SBP increased in the A and H+A groups, but GN was not induced in the A group. Therefore, GN in our model was induced not by HV or AII alone, but by the combination of HV and AII, independent of any increase in systemic blood pressure.

HIF-1α is a master transcriptional factor, transactivating the expression of many genes important for cell survival under hypoxic conditions [11–13, 26]. These genes are responsible for glycolysis, angiogenesis, proliferation and iron metabolism, all of which are induced by hypoxic stress; thus, the induction of HIF-1α is a marker of hypoxia. HIF-1α is regulated at the post-translational level by the proteasome system through ubiquitination with von Hippel-Lindau (VHL) protein [27, 28]. As previously reported, this regulation of HIF-1α protein level is dependent on the concentration of oxygen. Hypoxia induces enhancement of HIF-1α protein stability leading to the elevation of the protein level due to inhibition of degradation by VHL. Therefore, hypoxia induces adaptation in cells including induction of HIF-1α; the hypoxic pathway. On the other hand, a line of evidence recently accumulated suggests that HIF-1α is also regulated independently of oxygen concentration through the nonhypoxic pathway [14, 15]. AII is reported to regulate HIF-1α both at transcriptional and post-translational levels in vascular smooth muscle cells cultured under normoxic condition through the AII type 1 receptor [14, 15]. Moreover, HIF-1α is also post-translationally regulated in several cell lines in the presence of tumor necrosis factor-α or nitric oxide independent of oxygen contents [29, 30].

As demonstrated in this study, immunoreactivity of HIF-1α was not detected in the N group (no treatment group), but HIF-1α was detected in the nuclei of glomerular, tubular and epithelial cells of the papilla by administration of AII alone or AII and HV together. This is the first evidence showing that HIF-1α was detected in the kidney by AII, independent of systemic hypoxic stress. As indicated here, HIF-1α was found to be expressed only in intact, not damaged glomeruli. Even within a glomerulus, only the intact part of glomerular cells expressed HIF-1α. Considering the fact that induction of HIF-1α is one of the defense mechanisms for cell survival [31–33], our data indicate that induction of HIF-1α is a marker of glomeruli survival; indeed, it could be a marker of renal protection.

To further investigate whether HIF-1α is involved in the progression or protection of GN, preinduction of HIF-1α was performed with $CoCl_2$ before administration of HV and AII. Surprisingly, the induction of HIF-1α by $CoCl_2$ pretreatment attenuated the progression of GN; the level of GN was reduced from 44.9 to 12.2% and the incidence of GN was reduced from 100 to 36.4%. Furthermore, as indicated, the preinduction of HIF-1α actually affects the inhibition of GN, because the rate of HIF-1α induction was parallel with that of the attenuation of GN. Therefore, our data suggest that HIF-1α is involved, at least in part, in the defense mechanism against the progression of GN, and hence could be a marker for renal protection.

AII is reported to induce HIF-1α [14, 15] and plays a partial role in the renal protective effect; however, the other effects of AII, such as increasing glomerular pressure and modulating gene expression involving in the renal

failure, may overcome any protective effect of AII-induced HIF-1α, and so as a result it may lead to the progression of GN.

In conclusion, we developed a highly reproducible GN model by combining HV and AII. Preinduction of HIF-1α remarkably attenuated the progression of GN, indicating that HIF-1α was involved in the defense mechanism of the kidney.

Acknowledgments

This work was supported by Grants-in-Aid for Scientific Research from the Ministry of Education, Science and Culture (No. 14657409). We thank Dr. Masami Nakatani, Dr. Noriko Kishimoto, Dr. Ichiro Yamasaki, Dr. Yoshitaka Kumon, Dr. Hiroaki Takeuchi, Dr. Jun Imamura, Dr. Mikio Kamioka, Ms. Chiaki Kawada, Ms. Chizuko Sugimoto, and Mr. Takuya Yamaguchi for their helpful advice and generous support.

References

1 Rifai A, Small PA Jr, Teague PO, Ayoub EM: Experimental IgA nephropathy. J Exp Med 1979;150:1161–1173.
2 Ishizaki M, Masuda Y, Fukuda Y, Yamanaka N, Masugi Y, Shichinohe K, Nakama K: Renal lesions in a strain of spontaneously diabetic WBN/Kob rats. Acta Diabetol Lat 1987;24:27–35.
3 Banks KL: Glomerulonephritis, autoimmunity, autoantibody. Animal model: Anti-glomerular basement membrane antibody in horses. Am J Pathol 1979;94:443–446.
4 Elzinga LW, Rosen S, Bennett WM: Dissociation of glomerular filtration rate from tubulointerstitial fibrosis in experimental chronic cyclosporine nephropathy: Role of sodium intake. J Am Soc Nephrol 1993;4:214–221.
5 Arendshorst WJ, Finn WF, Gottschalk CW: Pathogenesis of acute renal failure following temporary renal ischemia in the rat. Circ Res 1975;37:558–568.
6 Wilson CB, Dixon FJ: Immunopathologic mechanisms of renal disease. Ric Clin Lab 1975;5:17–38.
7 Masuda Y, Shimizu A, Mori T, Ishiwata T, Kitamura H, Ohashi R, Ishizaki M, Asano G, Sugisaki Y, Yamanaka N: Vascular endothelial growth factor enhances glomerular capillary repair and accelerates resolution of experimentally induced glomerulonephritis. Am J Pathol 2001;159:599–608.
8 Kim S, Iwao H: Molecular and cellular mechanisms of angiotensin II-mediated cardiovascular and renal diseases. Pharmacol Rev 2000;52:11–34.
9 Lee LK, Meyer TW, Pollock AS, Lovett DH: Endothelial cell injury initiates glomerular sclerosis in the rat remnant kidney. J Clin Invest 1995;96:953–964.
10 Huang LE, Arany Z, Livingston DM, Bunn HF: Activation of hypoxia-inducible transcription factor depends primarily upon redox-sensitive stabilization of its alpha subunit. J Biol Chem 1996;271:32253–32259.
11 Wang, GL, Jiang BH, Rue EA, Semenza GL: Hypoxia-inducible factor 1 is a basic-helix-loop-helix-PAS heterodimer regulated by cellular O_2 tension. Proc Natl Acad Sci USA 1995;92:5510–5514.
12 Rosenberger C, Mandriota S, Jurgensen JS, Wiesener MS, Horstrup JH, Frei U, Ratcliffe PJ, Maxwell PH, Bachmann S, Eckardt KU: Expression of hypoxia-inducible factor-1alpha and -2alpha in hypoxic and ischemic rat kidneys. J Am Soc Nephrol 2002;13:1721–1732.
13 Wenger RH, Rolfs A, Marti HH, Guenet JL, Gassmann M: Nucleotide sequence, chromosomal assignment and mRNA expression of mouse hypoxia-inducible factor-1 alpha. Biochem Biophys Res Commun 1996;223:54–59.
14 Richard DE, Berra E, Pouyssegur J: Nonhypoxic pathway mediates the induction of hypoxia-inducible factor 1alpha in vascular smooth muscle cells. J Biol Chem 2000;275:26765–26771.
15 Page EL, Robitaille GA, Pouyssegur J, Richard DE: Induction of hypoxia-inducible factor-1alpha by transcriptional and translational mechanisms. J Biol Chem 2002;277:48403–48409.
16 Raij L, Azar S, Keane W: Mesangial immune injury, hypertension, and progressive glomerular damage in Dahl rats. Kidney Int 1984;26:137–143.
17 Linas SL, Shanley PF, Whittenburg D, Berger E, Repine JE: Neutrophils accentuate ischemia-reperfusion injury in isolated perfused rat kidneys. Am J Physiol 1988;255:F728–F735.
18 Romero F, Rodriguez-Iturbe B, Parra G, Gonzalez L, Herrera-Acosta J, Tapia E: Mycophenolate mofetil prevents the progressive renal failure induced by 5/6 renal ablation in rats. Kidney Int 1999;55:945–955.
19 Kaneko Y, Shiozawa S, Hora K, Nakazawa K: Glomerulosclerosis develops in Thy-1 nephritis under persistent accumulation of macrophages. Pathol Int 2003;53:507–517.
20 Barnes JL, Lisa MS: Origin of interstitial fibroblasts in an accelerated model of angiotensin II (AII)-induced interstitial fibrosis. J Am Soc Nephrol 2001;12:699A3645.
21 Cattell V, Bradfield JW: Focal mesangial proliferative glomerulonephritis in the rat caused by habu snake venom. A morphologic study. Am J Pathol 1977;87:511–524.
22 Kitamura H, Sugisaki Y, Yamanaka N: Endothelial regeneration during the repair process following Habu-snake venom induced glomerular injury. Virchows Arch 1995;427:195–204.
23 Ruggenenti P: Angiotensin-converting enzyme inhibition and angiotensin II antagonism in nondiabetic chronic nephropathies. Semin Nephrol 2004;24:158–167.
24 Tolins JP, Raij L: Effects of amino acid infusion on renal hemodynamics. Role of endothelium-derived relaxing factor. Hypertension 1991;17:1045–1051.
25 Nakamura T, Obata J, Kimura H, Ohno S, Yoshida Y, Kawachi H, Shimizu F: Blocking angiotensin II ameliorates proteinuria and glomerular lesions in progressive mesangioproliferative glomerulonephritis. Kidney Int 1999;55:877–889.
26 Makino Y, Cao R, Svensson K, Bertilsson G, Asman M, Tanaka H, Cao Y, Berkenstam A, Poellinger L: Inhibitory PAS domain protein is a negative regulator of hypoxia-inducible gene expression. Nature 2001;414:550–554.
27 Neckers LM: aHIF: The missing link between HIF-1 and VHL? J Natl Cancer Inst 1999;91:106–107.
28 Maxwell PH, Wiesener MS, Chang GW, Clifford SC, Vaux EC, Cockman ME, Wykoff CC, Pugh CW, Maher ER, Ratcliffe PJ: The tumour suppressor protein VHL targets hypoxia-inducible factors for oxygen-dependent proteolysis. Nature 1999;399:271–275.
29 Zhou J, Fandrey J, Schumann J, Tiegs G, Brune B: NO and TNF-alpha released from activated macrophages stabilize HIF-1alpha in resting tubular LLC-PK1 cells. Am J Physiol Cell Physiol 2003;284:C439–C446.
30 Sandau KB, Zhou J, Kietzmann T, Brune B: Regulation of the hypoxia-inducible factor 1alpha by the inflammatory mediators nitric oxide and tumor necrosis factor-alpha in contrast to desferroxamine and phenylarsine oxide. J Biol Chem 2001;276:39805–39811.
31 Prass K, Ruscher K, Karsch M, Isaev N, Megow D, Priller J, Scharff A, Dirnagl U, Meisel A: Desferrioxamine induces delayed tolerance against cerebral ischemia in vivo and in vitro. J Cereb Blood Flow Metab 2002;22:520–525.
32 Furuta GT, Turner JR, Taylor CT, Hershberg RM, Comerford K, Narravula S, Podolsky DK, Colgan SP: Hypoxia-inducible factor 1-dependent induction of intestinal trefoil factor protects barrier function during hypoxia. J Exp Med 2001;193:1027–1034.
33 Matsumoto M, Makino Y, Tanaka T, Tanaka H, Ishizaka N, Noiri E, Fujita T, Nangaku M: Induction of renoprotective gene expression by cobalt ameliorates ischemic injury of the kidney in rats. J Am Soc Nephrol 2003;14:1825–1832.

循環器科，58(6)：600-605，2005

特集 先駆的医工学と循環器

バイオニック動脈圧反射による血圧コントロール*

佐藤隆幸**

Key Words : arterial pressure, baroreflex failure, bionics, orthostatic hypotension, sympathetic nerve

はじめに

最近の老年医学研究により，加齢に伴う動脈圧反射障害が起立性低血圧をひき起こし，廃用症候群(いわゆる寝たきり)の重要な誘因であることが明らかになりつつある．また，中高年を好発年齢とする進行性の神経変性疾患，たとえば，シャイ・ドレーガー症候群・多系統萎縮症，あるいは，外傷による高位脊髄損傷などでは，生命維持にきわめて重要な血管運動中枢が侵されたり，交感神経遠心路障害により圧反射機能が廃絶するため，重度の起立性低血圧や起立性失神を起こすようになる．多くの場合，最終的には寝たきり状態となる[1)~3)]．

このように起立性低血圧は，生活の質を著しく低下させる重要な病態であるが，多くの場合，根治的治療法はない．これまでに，薬物療法と心臓ペースメーカによる頻拍ペーシングが試されてきたがいずれも無効であった[4)5)]．血管収縮剤やミネラルコルチコイドによる薬物療法の場合，仮に，起立時の低血圧を防止することに成功しても，臥位時の重症高血圧をまねくことがあった．また，頻拍ペーシングは動脈圧調節の前負荷(中心静脈圧)依存性を増強し，むしろ起立性低血圧を悪化させることがあった．このようなことから，ヒトの体位変換時の血圧調節に絶対的に重要な圧反射機能を再建することこそが治療の唯一の方法であると認識されるようになってきた．

そこで著者らは，圧反射機能を再建する医工学的アプローチとしてバイオニック圧反射装置を開発し，その有効性を術中の起立性低血圧モデルで検証し，臨床応用への道を模索している[6)~8)]．

バイオニック動脈圧反射装置の開発

1．開発の原理

動脈圧反射は，さまざまな外乱による脳の灌流圧変化を抑制する機構としてはたらくきわめて重要なフィードバック制御システムである[9)~11)]．時々刻々と変化する動脈圧は，頸動脈洞や大動脈弓の圧受容器で検知され，圧受容器神経活動として血管運動中枢にフィードバックされる．血管運動中枢はこの圧受容器神経活動に応じて，交感神経活動を変化させる．その結果，血管の収縮・弛緩が生じ，外乱の影響が抑制されることになる．したがって，動脈圧反射は，重力環境下での臥位から立位への体位変換時の血圧低下，すなわち起立性低血圧を防止する血圧制御機構として必須である．動脈圧反射失調では，

* Bionic baroreflex control of arterial pressure.

** Takayuki SATO, M.D., Ph.D.: 高知大学医学部循環制御学教室〔〒783-8505 南国市岡豊町小蓮〕; Department of Cardiovascular Control, Kochi Medical School, Nankoku 783-8505, JAPAN

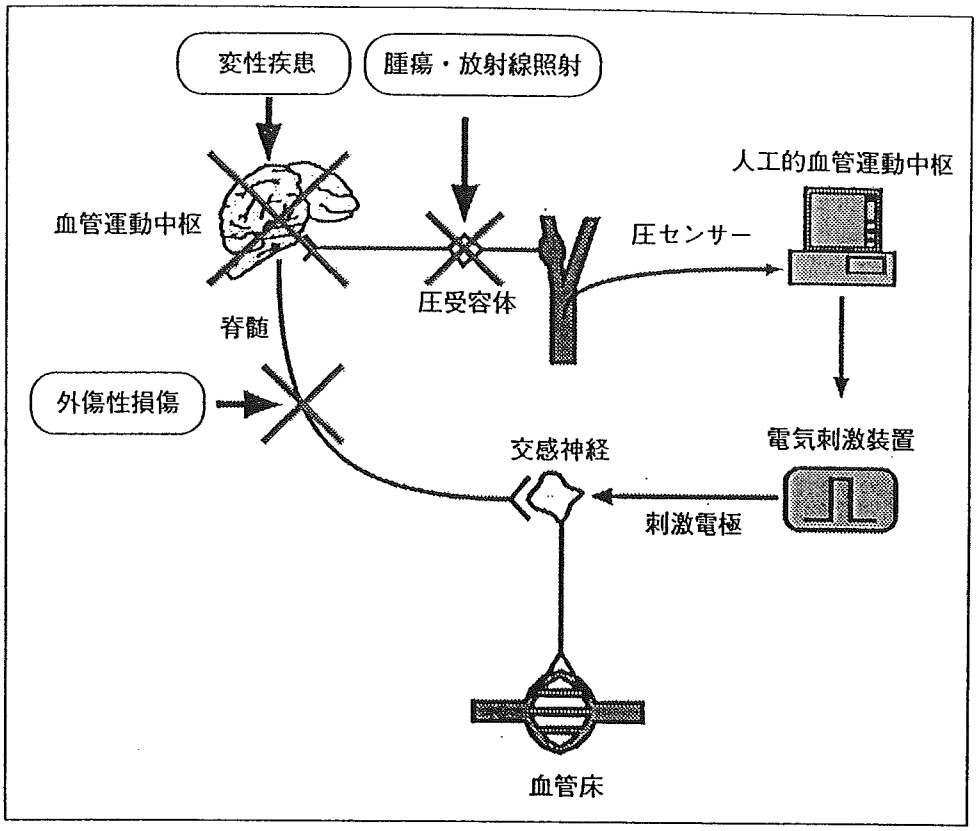

図1　動脈圧反射障害をきたす病態とバイオニック動脈圧反射装置

これら一連の反射性血圧調節が作動しないため，起立性低血圧が必発となる．したがって，このような患者を救うためには，機能廃絶した血管運動中枢の機能代行装置として，人工的血管運動中枢を有した血圧制御装置が必要となる．

バイオニック動脈圧反射装置の動作原理は，図1のように，「血圧を常時監視しながら，実時間演算で交感神経の電気刺激頻度を決定する」というものである．すなわち，本装置は，圧センサー→人工的血管運動中枢(コンピュータ)→電気刺激装置→交感神経→血管床からなるフィードバック血圧制御装置である[6)~8)]．

2．理論的背景[12)]

バイオニック動脈圧反射における情報の流れをブロック線図にすると図2のようになる．制御工学の分野で古典的に用いられる積分・比例補償型のフィードバック制御の理論を応用した．現在の血圧値の設定値からのずれにもとづいて交感神経の刺激頻度を決定する人工的血管運動中枢，すなわち制御部の伝達関数を$H_1(f)$とする．伝達関数は周波数領域での入出力関係を記述したものである．また，交感神経の刺激頻度の変化に対する血圧応答に関する効果器の伝達関数を$H_2(f)$とする．

現在の血圧値$AP(f)$の設定値$AP_t(f)$からのずれ$E(f)$は，

$$E(f)=AP_t(f)-AP(f) \quad \cdots\cdots (1)$$

と表される．$H_1(f)$は，比例補償係数K_pと積分補償係数K_iおよびラプラス演算子$s=2\pi fj$を用いると次のように表される．

$$H_1(f)=K_p+\frac{K_i}{s} \quad \cdots\cdots (2)$$

また，

$$STM(f)=E(f)\cdot H_1(f) \quad \cdots\cdots (3)$$

となる．

一方，現在の血圧値は，交感神経の刺激頻度の変化と外乱$AP_d(f)$によって変動することから，

$$AP(f)=STM(f)\cdot H_2(f)+AP_d(f) \quad \cdots (4)$$

最終的に，外乱の影響が現在の血圧値にどのように反映されるかは，式(1)，(3)，(4)を整頓して，

$$AP(f)=\frac{H_1(f)H_2(f)}{1+H_1(f)H_2(f)}AP_t(f)+\frac{1}{1+H_1(f)H_2(f)}AP_d(f)$$

となることから明らかなように，バイオニック

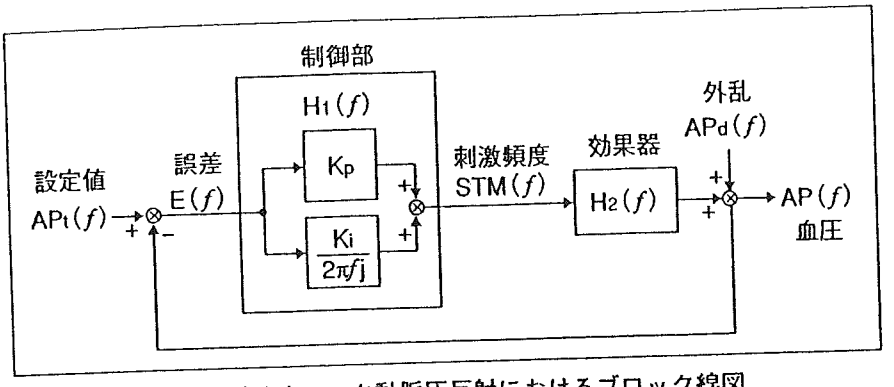

図2 バイオニック動脈圧反射におけるブロック線図
生体本来の動脈圧反射と同様に，バイオニック動脈圧反射では，血圧を乱そうとする外乱の影響を抑制して血圧の安定化をはかる．

動脈圧反射装置を用いたフィードバック制御により，$1/[1+H_1(f)H_2(f)]$に抑制されることがわかる．

以上のようなことから，バイオニック動脈圧反射装置が有効に働くようにするためには，式(2)におけるK_pとK_iが適切に決定されることが必要になる．具体的には，人工的血管運動中枢として働くコンピュータのプログラムが有効性の鍵を握っているということになる．

われわれは，$H_2(f)$を実験的臨床研究によって求め，K_pとK_iについては，数値シミュレーションによってもっとも有効に外乱の影響を抑えることが可能な値に決定し，$H_1(f)$を最適化した．

3．ヒトの交感神経刺激法と刺激に対する血圧の応答特性

これまでの動物実験や臨床研究から，胸腰髄レベルに留置した硬膜外カテーテル電極により，効率よく動脈圧を制御可能であることが判明している[6~8)13)~15)]．そこで，変形性頸椎症・頸椎椎間板ヘルニア・後縦靱帯骨化症などの手術時に術中脊髄機能モニタリングとして，脊髄誘発電位記録を行う患者を対象として，不規則に電気刺激を行いながら血圧応答を記録した．12例の患者からデータを取得し，$H_2(f)$を推定した．脊髄の刺激に応じて血圧が変動していることがわかる．

脊髄刺激頻度の変化を入力，血圧応答を出力として推定された伝達関数の結果を図3-Bに示す．平均的な伝達関数$H_2(f)$を求めるために，下記の二次の低域通過フィルターへの曲線近似法を用いて解析した．

$$H_2(f)=\frac{a}{1+2\zeta\left(\frac{f}{f_N}j\right)+\left(\frac{f}{f_N}j\right)^2}\exp(-2\pi f jL)$$

なお，aは定常ゲイン，ζは減衰係数，f_Nは固有周波数，Lはラグ時間である．その結果，それぞれ，0.4, 2.6, 0.06Hz, 9秒という結果が得られた．

4．人工的血管運動中枢の設計

近似$H_2(f)$を用いて，ステップ状の血圧低下(−20mmHg)に対するバイオニック動脈圧反射の振る舞いを比例補償係数K_p＝0, 1, 2，積分補償係数K_i＝0, 0.01, 0.05, 0.1, 0.2の組合わせでシミュレーションした．K_pとK_iの両者が0の場合には，外乱の影響はまったく圧縮されない(図4-A～Cの実線)．

K_p＝0の場合，全体的に血圧応答が緩徐である．K_iの増加に従い，立上がり時間(rise time, T_r)および整定時間(settling time, T_s)の短縮がみられるが，K_iが0.05を超えると不足減衰応答(under-damped response)がみられるようになり，動脈圧反射が不安定になってくる．

K_p＝2の場合，T_rは短く応答は迅速であるが，K_iの値にかかわらず動脈圧反射は不安定である．

K_p＝1の場合，動脈圧反射は，K_p＝0に比べ迅速で，K_iが0.1になるまでほとんど振動はみられない．K_i＝0.1のとき，T_rは約50秒で，T_sは60秒以内であった．動脈圧反射の迅速な応答と安定性の両者を満たすものとして，この付近の条件が適していると考えられた．

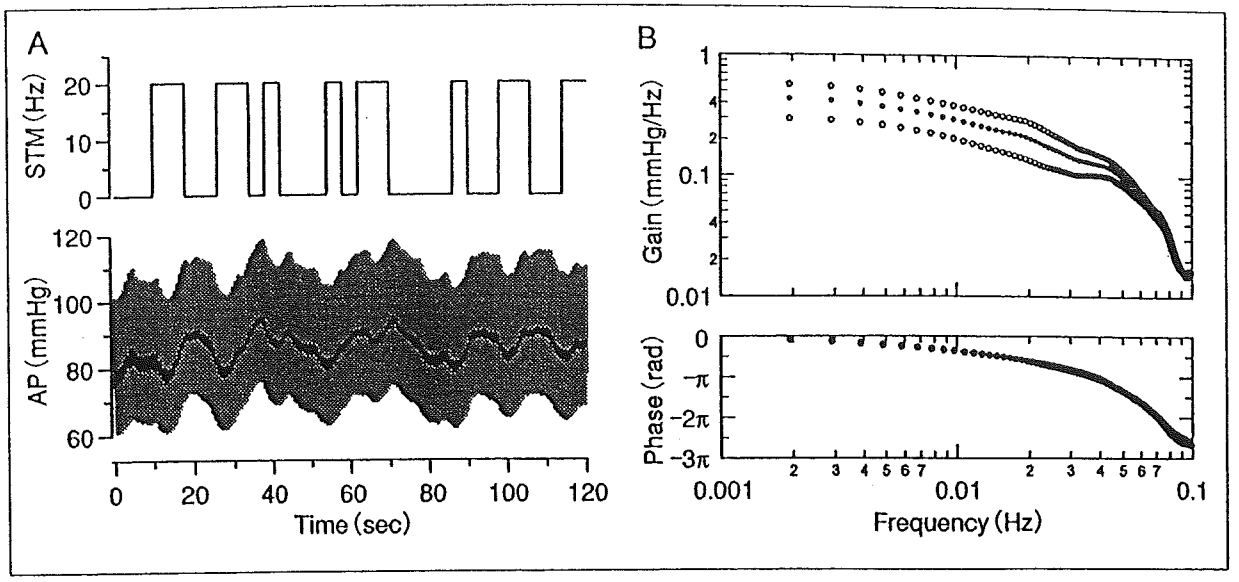

図3

A：不規則な脊髄交感神経刺激に対する血圧応答．刺激頻度(STM)を0か20ヘルツに不規則に変化させ，血圧応答(AP)を記録した．B：刺激頻度の変化に対する血圧応答の動的な特性を示す伝達関数．黒丸が平均値で白丸が平均±標準偏差(12例)を示す．

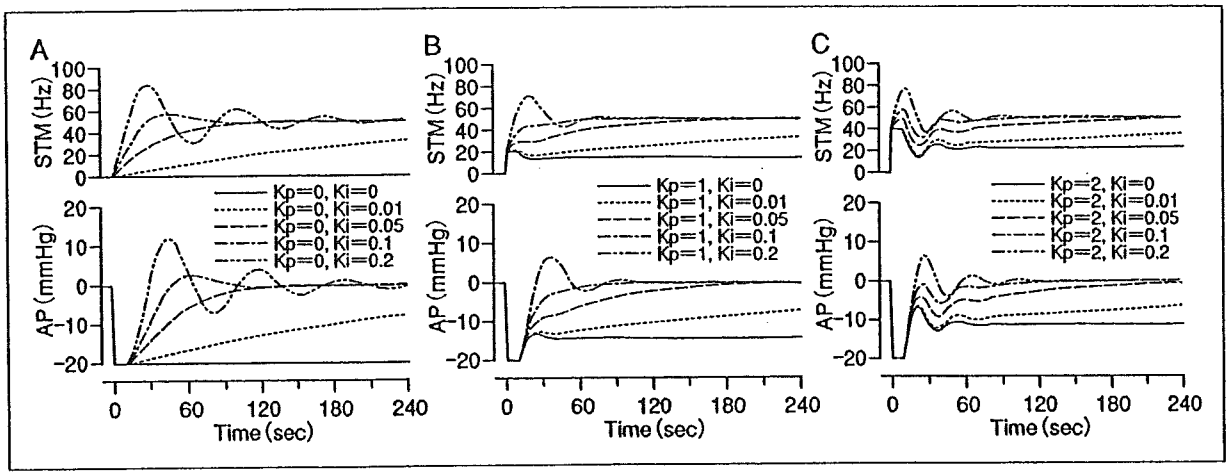

図4　人工的血管運動中枢の設計のためのシミュレーション

図2における比例補償係数(K_p)と積分補償係数(K_i)の組合わせを変えて，−20mmHgの外乱の影響がどのように表れるかを数値解析した．補償係数がともにゼロの場合には，外乱の影響はまったく抑制されない．

バイオニック動脈圧反射装置の有効性の検証

上記の結果を用いて，人工的血管運動中枢を設計し，試作したバイオニック動脈圧反射装置の有効性を検証した．検証にあたっては，起立性低血圧と同様，あるいは類似の血行動態変化による急激でかつ再現性のある低血圧モデルが理想的である．そこで，下肢人工関節置換術の際に止血目的で大腿部に圧迫帯を用いる症例に着目した．このような症例では，圧迫帯の解除時に急激な低血圧を生ずることが知られている[16)17)]．バイオニック動脈圧反射装置の作動中に圧迫解除を行った場合と，そうでない場合で，血圧がどのように変化するかを検討した．22例から得られた結果は，図5に示されている．大腿部の圧迫止血帯の急速解除に伴う血行動態は，解除後急激に血圧と中心静脈圧が低下した．これは，圧迫解除に伴う下肢への血液貯留により静脈還流が減少し心拍出量が減少したことと，大腿動脈の圧迫解除によって血管床の相対的増加がもたらされ，血管抵抗が減少したことを示

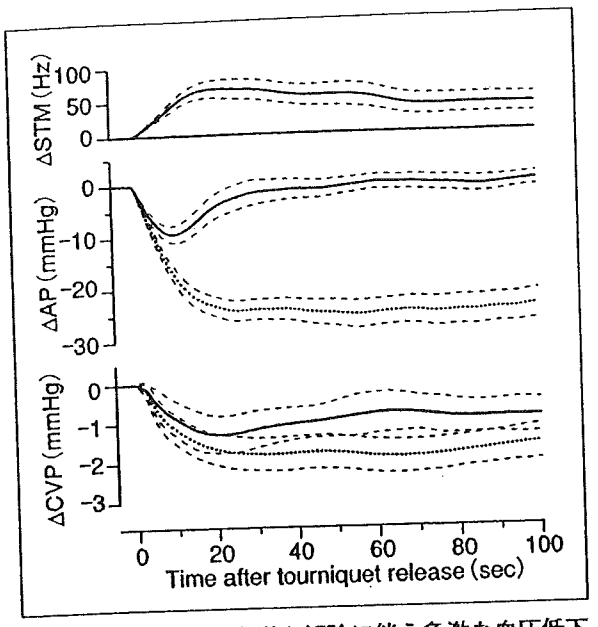

図5 圧迫止血帯の急激な解除に伴う急激な血圧低下
バイオニック動脈圧反射装置が作動していない場合(点線)には，圧迫止血帯の解除に伴い急激に血圧(AP)と中心静脈圧(CVP)が低下したが，バイオニック動脈圧反射が作動している場合(実線)には，両者ともに低下が抑制された．破線は平均±標準偏差(22例)を示す．

唆している．したがって，このような，10秒以内に血圧が20mmHg低下するモデルは，バイオニック動脈圧反射装置の有効性を評価するために妥当であると考えられた．

図から明らかなように，バイオニック動脈圧反射装置が作動している場合には，圧迫止血帯の解除に伴う急激な血圧低下は，数秒以内に食い止められ，止血帯解除前の血圧値にすみやかに回復した．以上のような結果から，バイオニック動脈圧反射装置は，本モデルのような血圧低下に対しては有用であると考えられた．

まとめ

起立性低血圧などのような血圧調節障害に対する治療法として，輸液・輸血法，薬物療法，機械的サポート法などが知られているが，本稿で紹介した手法はこれらとは異なり，自律神経系とインターフェイスして，医工学的に動脈圧反射機能を再建しようとするものである．その利点は，神経性であるがゆえに迅速な調節が可能であるだけでなく，オンデマンド的動作であるため，不要な臥位高血圧をまねく危険性が少ないことも期待される．

バイオニック動脈圧反射装置を臨床応用するにあたっては，長期使用の可能な交感神経刺激電極の開発や小型電気刺激装置が必要となるが，すでに難治性てんかんの治療用としてカフ型の迷走神経刺激電極や刺激装置が開発され，多くの症例に使用されている[18]．したがって，このような要素技術を応用すれば，バイオニック動脈圧反射装置が起立性低血圧の治療器として実用化できるかもしれない．

文　献

1) Robertson D. Diagnosis and management of baroreflex failure. Primary Cardiol 1995 ; 21 : 37.
2) The Consensus Committee of the American Autonomic Society and the American Academy of Neurology. Consensus statement on the definition of orthostatic hypotension, pure autonomic failure, and multiple system atrophy. Neurology 1996 ; 46 : 1470.
3) Ketch T, Biaggioni I, Robertson R, et al. Four faces of baroreflex failure : hypertensive crisis, volatile hypertension, orthostatic tachycardia, and malignant vagotonia. Circulation 2002 ; 105 : 2518.
4) Bannister R, da Costa DF, Hendry WG, et al. Atrial demand pacing to protect against vagal overactivity in sympathetic autonomic neuropathy. Brain 1986 ; 109 : 345.
5) Kristinsson A. Programmed atrial pacing for orthostatic hypotension. Acta Med Scand 1983 ; 214 : 79.
6) Sato T, Kawada T, Shishido T, et al. Novel therapeutic strategy against central baroreflex failure : a bionic baroreflex system. Circulation 1999 ; 100 : 299.
7) Sato T, Kawada T, Sugimachi M, et al. Bionic technology revitalizes native baroreflex function in rats with baroreflex failure. Circulation 2002 ; 106 : 730.
8) Yanagiya Y, Sato T, Kawada T, et al. Bionic epidural stimulation restores arterial pressure regulation during orthostasis. J Appl Physiol 2004 ; 97 : 984.
9) Guyton AC, Coleman TG, Granger HJ. Circulation : overall regulation. Ann Rev Physiol 1972 ; 34 : 13.
10) Sato T, Kawada T, Inagaki M, et al. New analytic

framework for understanding sympathetic baroreflex control of arterial pressure. Am J Physiol Heart Circ Physiol 1999 ; 276 : H2251.

11) Sunagawa K, Sato T, Kawada T. Integrative sympathetic baroreflex regulation of arterial pressure. Ann NY Acad Sci 2001 ; 940 : 314.

12) Kawada K, Sunagawa G, Takaki H, et al. Development of a servo-controller of heart rate using a treadmill. Jpn Circ J 1999 ; 63 : 945.

13) Hainsworth R, Karim F. Responses of abdominal vascular capacitance in the anaesthetized dog to changes in carotid sinus pressure. J Physiol (Lond) 1976 ; 262 : 659.

14) Carneiro JJ, Donald DE. Blood reservoir function of dog spleen, liver, and intestine. Am J Physiol Heart Circ Physiol 1977 ; 232 : H67.

15) Minson CT, Wladkowski SL, Pawelczyk JA, et al. Age, splanchnic vasoconstriction, and heat stress during tilting. Am J Physiol Regul Integr Comp Physiol 1999 ; 276 : R203.

16) Kahn RL, Marino V, Urquhart B, et al. Hemodynamic changes associated with tourniquet use under epidural anesthesia for total knee arthroplasty. Reg Anesth 1992 ; 17 : 228.

17) Sander-Jensen K, Mehlsen J, Secher NH, et al. Progressive central hypovolaemia in man–resulting in a vasovagal syncope? Haemodynamic and endocrine variables during venous tourniquets of the thighs. Clin Physiol 1987 ; 7 : 231.

18) Reid SA. Surgical technique for implantation of the neurocybernetic prosthesis. Epilepsia 1990 ; 31 Suppl 2 : S38.

* * *

Artificial Baroreflex

Clinical Application of a Bionic Baroreflex System

Fumiyasu Yamasaki, MD; Takahiro Ushida, MD; Takeshi Yokoyama, DDS; Motonori Ando, PhD; Koichi Yamashita, MD; Takayuki Sato, MD

Background—We proposed a novel therapeutic strategy against central baroreflex failure: implementation of an artificial baroreflex system to automatically regulate sympathetic vasomotor tone, ie, a bionic baroreflex system (BBS), and we tested its efficacy in a model of sudden hypotension during surgery.

Methods and Results—The BBS consisted of a computer-controlled negative-feedback circuit that sensed arterial pressure (AP) and automatically computed the frequency (STM) of a pulse train required to stimulate sympathetic nerves via an epidural catheter placed at the level of the lower thoracic spinal cord. An operation rule was subsequently designed for the BBS using a feedback correction with proportional and integral gain factors. The transfer function from STM to AP was identified by a white noise system identification method in 12 sevoflurane-anesthetized patients undergoing orthopedic surgery involving the cervical vertebrae, and the feedback correction factors were determined with a numerical simulation to enable the BBS to quickly and stably attenuate an external disturbance on AP. The performance of the designed BBS was then examined in a model of orthostatic hypotension during knee joint surgery (n=21). Without the implementation of the BBS, a sudden deflation of a thigh tourniquet resulted in a 17±3 mm Hg decrease in AP within 10 seconds and a 25±2 mm Hg decrease in AP within 50 seconds. By contrast, during real-time execution of the BBS, the decrease in AP was 9±2 mm Hg at 10 seconds and 1±2 mm Hg at 50 seconds after the deflation.

Conclusions—These results suggest the feasibility of a BBS approach for central baroreflex failure. **(*Circulation*. 2006; 113:634-639.)**

Key Words: baroreceptors ■ blood pressure ■ computers ■ electrical stimulation ■ nervous system, sympathetic

The arterial baroreflex acts to maintain cerebral perfusion by quickly attenuating the effect of an external disturbance, such as the assumption of an upright position, on arterial pressure (AP).[1–4] Therefore, functional restoration of dynamic properties of the arterial baroreflex is essential for the treatment of patients with various syndromes of baroreflex failure,[5] including Shy-Drager syndrome,[6–9] baroreceptor deafferentation,[10,11] and traumatic spinal cord injuries.[12,13] However, most commonly used interventions, including salt loading,[14,15] cardiac pacing,[16,17] and adrenergic agonists,[18,19] can neither restore nor reproduce the functioning of the native vasomotor center, and most affected patients remain bedridden.

Clinical Perspective p 639

We recently developed a framework for identifying an operational rule of the vasomotor center and a prototype of a bionic baroreflex system (BBS) in rats.[20–22] The BBS consisted of a negative-feedback system controlled by a computer (ie, the artificial vasomotor center) that sensed AP and automatically computed the frequency of a pulse train required to stimulate sympathetic efferent nerves through a pair of wire electrodes placed in the celiac ganglion. Previous experimental work demonstrated that the BBS restored native baroreflex function in rats with central baroreflex failure; however, an applicable neural interface with quick and effective controllability of AP is required for application of this technology in the clinical setting. The goal of the present study was to determine the efficacy of a novel bionic technology for the intraoperative restoration of AP in the context of central baroreflex failure and to validate this technology in a clinical model of orthostatic hypotension.

Methods

All studies were approved by the institutional review committee, and all subjects gave informed consent.

Theoretical Considerations

As previously described,[20–22] the principle of the BBS is based on a negative-feedback mechanism (Figure 1). The instantaneous AP is measured by a pressure transducer connected to a computer that functions as a controller or artificial vasomotor center. Instead of the disabled native vasomotor center, the controller automatically exe-

Received September 8, 2005; revision received October 31, 2005; accepted November 21, 2005.

From the Departments of Cardiovascular Control (F.Y., M.A., T.S.), Clinical Laboratory (F.Y.), Orthopedic Surgery (T.U.), and Anesthesiology (T.Y., K.Y.), Kochi Medical School, Nankoku, Japan.

Correspondence to Fumiyasu Yamasaki, MD, Department of Clinical Laboratory, Kochi Medical School, Nankoku 783-8505, Japan. E-mail yamasakf@med.kochi-u.ac.jp

Circulation **is available at http://www.circulationaha.org**

DOI: 10.1161/CIRCULATIONAHA.105.587915

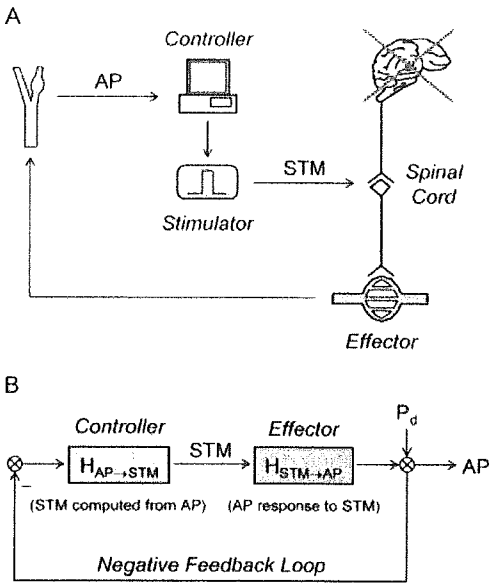

Figure 1. Schematic illustration (A) and block diagram (B) of a BBS. In the context of central baroreflex failure, the BBS automatically computes the frequency (STM) of a pulse train to stimulate sympathetic nerves through an epidural catheter placed at the level of lower thoracic spinal cord, while simultaneously sensing the change in AP. $H_{AP\rightarrow STM}$ denotes a transfer function for the controller functioning as an artificial vasomotor center. $H_{STM\rightarrow AP}$ is a transfer function showing the dynamic response of AP to STM. The overall transfer function of the BBS is given by $H_{AP\rightarrow STM}\times H_{STM\rightarrow AP}$. Therefore, the effect of an external disturbance (P_d) on AP is attenuated to $1/(1+H_{AP\rightarrow STM}\times H_{STM\rightarrow AP})$.

cutes real-time operations that determine the frequency of electrical stimulation (STM) required to minimize the effect of an external disturbance (P_d) on AP and then commands an electrical stimulator to deliver a stimulus of the same frequency to the vasomotor sympathetic nerves via epidural-catheter electrodes placed at the lower thoracic level of the spinal cord. The lower thoracic level was selected as the site for the neural interface of the BBS because the abdominal splanchnic vascular bed is a major effector mechanism for the arterial baroreflex.[23–25]

According to a classic feedback-control theory, ie, feedback correction with proportional and integral gain factors,[26,27] the following algorithm was used to program the controller for the calculation of STM in the frequency domain:

$$H_{AP\rightarrow STM}=K_p+\frac{K_i}{2\pi fj} \quad (1)$$

where $H_{AP\rightarrow STM}$ is a transfer function from AP to STM, K_p is the proportional correction factor, K_i is the integral correction factor, and j is the imaginary unit. The proportional factor determines the feedback amplification based on the absolute value of the instantaneous control error due to P_d, and the integral factor adjusts the feedback amplification based on the cumulative value of the instantaneous control error. Therefore, STM is computed as follows:

$$STM=-AP\cdot H_{AP\rightarrow STM} \quad (2)$$

and AP is also expressed as follows:

$$AP=STM\cdot H_{STM\rightarrow AP}+P_d \quad (3)$$

where $H_{STM\rightarrow AP}$ denotes the frequency response of AP to STM. From Equations 2 and 3, the effect of P_d on AP is estimated as follows:

$$AP=\frac{1}{1+H_{AP\rightarrow STM}\cdot H_{STM\rightarrow AP}}P_d \quad (4)$$

Thus, if $H_{AP\rightarrow STM}\cdot H_{STM\rightarrow AP}$ is far larger than unity, the BBS can nullify the effect of P_d on AP.

Subjects and Experimental Protocols

A total of 33 patients (46 to 84 years old, 19 males) who underwent orthopedic operations were enrolled in the present study. Ten patients had hypertension, and 4 had diabetes mellitus. None of the subjects had frequent ectopic beats or atrial fibrillation. After induction anesthesia with propofol, an endotracheal tube was introduced orally. The patients were mechanically ventilated with 67% nitrous oxide and 1.5% to 2% end-tidal sevoflurane in oxygen during experimental protocols, while end-tidal carbon dioxide was maintained at 35 to 38 mm Hg. An arterial catheter was placed in the radial artery for AP measurement. To record central venous pressure (CVP), a central venous catheter was placed in the femoral vein, and the tip of the catheter was advanced into the inferior vena cava just above the diaphragmatic level. Furthermore, an epidural catheter was placed percutaneously, and the tip, which contained a pair of electrodes (Unique Medical, Tokyo; interelectrode distance 15 mm), was placed at the level of Th_{9-11}. Placement of the central venous catheter and the epidural catheter was verified by chest radiograph.[28]

Before making an incision of affected areas, we performed 2 different protocols in separate groups of patients. In the first group of patients (n=12, 46 to 76 years old, 7 males) undergoing operations for cervical spondylosis and canal stenosis, the averaged $H_{STM\rightarrow AP}$ was estimated and the $H_{AP\rightarrow STM}$ was designed parametrically with Equation 1 to minimize the effect of P_d on AP. After we programmed the designed $H_{AP\rightarrow STM}$ into the computer, the efficacy of the BBS was tested against the rapid progressive hypotension induced by use of a thigh tourniquet[29–31] in the second group of patients (n=21, 64 to 84 years old, 12 males) undergoing operation for knee joint osteoarthritis. During each protocol, the muscle twitches induced by spinal cord stimulation were prevented by the intravenous administration of vecuronium bromide. Analgesia for the pain provoked by spinal cord stimulation and tourniquet inflation was provided by intravenous injection of fentanyl citrate. In a preliminary study, the validity of the analgesic preparation was confirmed for the experimental protocols, and the safety of spinal cord stimulation for 20 minutes was verified.

Estimation of Transfer Function From STM to AP

To characterize the dynamic nature of the AP response to STM, ie, $H_{STM\rightarrow AP}$, the lower thoracic sympathetic nerves were randomly stimulated for 15 minutes while we recorded AP. According to a white noise method for system identification, the STM was altered between 0 and 20 Hz every 4 seconds. The pulse width of electrical stimuli was fixed at 0.1 ms. The stimulation current was adjusted for each patient so as to produce a pressor response of ≈10 mm Hg at 20 Hz. This resulted in an average current of 15±4 (mean±SD) mA. The electrical signals of STM and AP were digitized at 100 Hz. As described previously,[20–22] the transfer function from STM to AP, $H_{STM\rightarrow AP}$, was estimated with a fast Fourier transform algorithm. Finally, the average of $H_{STM\rightarrow AP}$ among 12 patients was calculated.

Design of Artificial Vasomotor Center

With substitution of the averaged $H_{STM\rightarrow AP}$ for Equation 4, the instantaneous AP response to P_d was simulated numerically, and a stepwise decline with an amplitude of 20 mm Hg was imposed on the BBS. While the feedback parameters of $H_{AP\rightarrow STM}$, ie, K_p and K_i, were altered, the effect of the parameters on the AP response was investigated. Finally, the parameters that enabled the BBS to quickly and stably minimize the effect of P_d on AP were determined.

Efficacy of BBS in a Clinical Model of Transient Hypotension

The performance of the BBS was evaluated in a clinical model of rapid transient hypotension (n=21). Rapid hypotension was evoked by the sudden deflation of a thigh tourniquet, which is widely used to achieve bloodless dissection during total knee arthroplasty.[29–31] Acute hypotension immediately after tourniquet release is a well-

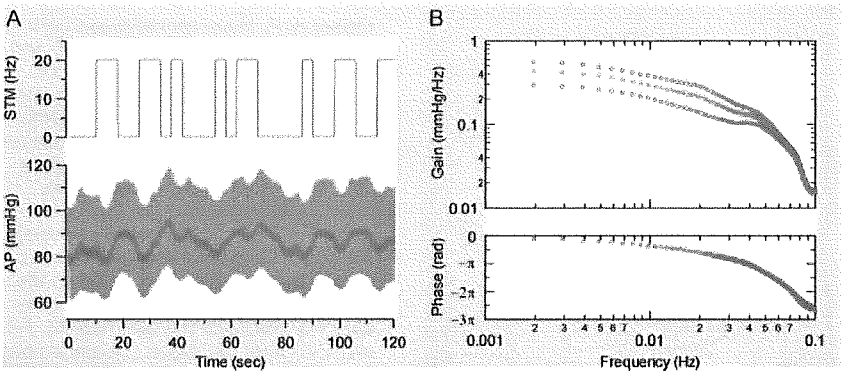

Figure 2. A, Representative example of time series data of the response of AP to random stimulation of the lower thoracic spinal cord. According to quasi-white noise, the STM was randomly altered between 0 and 20 Hz. The AP seems to slowly respond to STM with a delay. B, Transfer function of the AP response to the STM change. Data are expressed as mean±SD for 12 patients. rad indicates radians. See text for explanation.

known phenomenon that results from a rapid decrease in peripheral vascular resistance and an increase in venous pooling in the affected limb.[29] The degree of hypotension can be potentiated by the use of volatile anesthetic agents such as sevoflurane, which are central depressants of arterial baroreflex function.[32,33] Therefore, tourniquet-related hypotension during sevoflurane anesthesia can be used as a model of orthostatic hypotension in central baroreflex failure.

Briefly, a tourniquet was applied to the upper femur and inflated at 300 mm Hg for 60 minutes and then quickly deflated for 10 minutes. The procedure was then repeated. The BBS was activated during 1 of the 2 trials of tourniquet-related hypotension, and the electrical signals of STM, CVP, and AP were digitized at 100 Hz.

Statistical Analysis

The hemodynamic responses to tourniquet release were measured for each subject while the BBS was being activated and inactivated. The effects of the BBS execution on the hemodynamic changes at 10, 50, and 100 seconds after tourniquet release were analyzed by paired *t* tests with Bonferroni adjustment. Differences were considered significant at overall $P<0.05$.

Results

A representative example of original tracings of STM and AP during random stimulation of the spinal cord is shown in Figure 2A. Random on-off change in STM produced a delayed and slow change in AP. The relationship between STM and AP was quantitatively characterized by the frequency domain analysis (Figure 2B). The averaged transfer function from STM to AP, $H_{STM\rightarrow AP}$, had low-pass characteristics with a corner frequency of 0.06 Hz. The gain factor was 0.43 ± 0.13 mm Hg · Hz^{-1} at the steady state (lowest frequency) and gradually decreased with input frequency. The phase spectrum showed that the input-output relationship was in phase and that the phase delay increased toward higher frequencies. The squared coherence, a measure of linear dependence between STM and AP, was >0.9 in the frequency range of interest (data not shown).

The results of simulation for the design of the artificial vasomotor center, $H_{AP\rightarrow STM}$, are presented in Figure 3. The AP responses to the external disturbance P_d were simulated under 12 different combinations with feedback correction factors. Without feedback compensation, ie, when both feedback correction factors were zero, there was no attenuation of the effect of the external disturbance on AP. Therefore, AP fell by 20 mm Hg immediately after the imposition of P_d (Figure 3A, black line). By contrast, if either or both of the correction factors were too large, the underdamped oscillatory response of AP appeared, and the BBS became unstable. On the basis of these results, K_p was set at 1, and K_i was set at 0.1, so that the BBS could quickly and effectively attenuate the effect of the external disturbance (Figure 3B, red line).

A representative example of the results of the performance tests of the BBS is shown in Figure 4A. A sudden

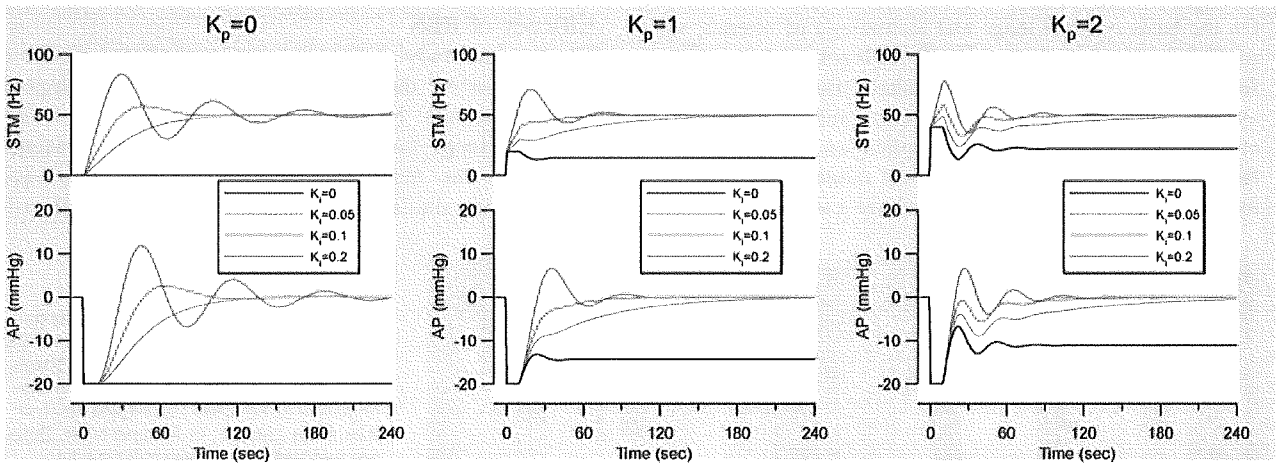

Figure 3. Numerical simulations of a feedback controller of the BBS. A stepwise pressure decline with an amplitude of 20 mm Hg is assumed to be imposed. Results are shown for 12 combinations of proportional (K_p) and integral (K_i) correction factors. See text for explanation.

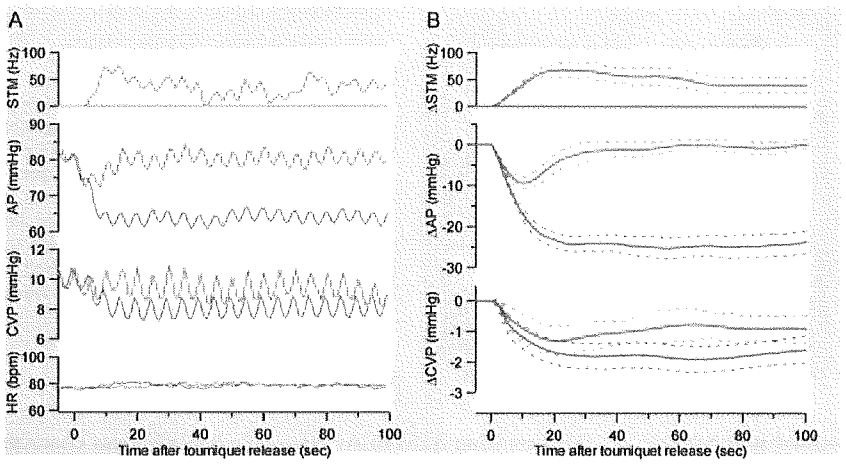

Figure 4. A, Representative example of original tracings of STM, AP, CVP, and heart rate (HR) during 2 episodes of rapid progressive hypotension induced by sudden deflation of a thigh tourniquet in a patient. When the BBS was inactive (blue line), AP decreased immediately after tourniquet release and did not return to baseline level. By contrast, when the BBS was activated (red line), the artificial vasomotor center automatically computed STM and drove an electrical stimulator to restore AP. B, Plots showing averaged changes in STM, AP, and CVP after tourniquet release among 21 patients. Data are expressed as mean (solid line)±SD (dotted line). See text for explanation.

deflation of the thigh tourniquet produced a rapid progressive fall in AP of ≈20 mm Hg within 10 seconds, while lowering CVP by 2 mm Hg. By contrast, when the BBS was activated, STM was computed automatically, and the spinal cord was stimulated appropriately to quickly and effectively attenuate the drop in AP and CVP. Figure 4B summarizes the results obtained from 21 patients, demonstrating effectiveness of the BBS performance in buffering the AP fall in response to the sudden release of the tourniquet. As demonstrated in Figure 5, tourniquet release resulted in an AP decrease of 17±3 mm Hg at 10 seconds, 25±2 mm Hg at 50 seconds, and 24±3 mm Hg at100 seconds. By contrast, during real-time execution of the BBS, the decrease in AP was 9±2 mm Hg at 10 seconds, 1±2 mm Hg at 50 seconds, and 0±1 mm Hg at 100 seconds after the deflation. These data indicated that the BBS significantly attenuated the decrease in AP at these 3 time points and nullified the hypotensive effect of tourniquet release within 50 seconds. Similarly, the BBS significantly suppressed the decrease in CVP within 50 seconds after the release of the tourniquet.

Discussion

Design of BBS

On the basis of knowledge and technology of bionics, we previously developed an artificial feedback control system for automatic regulation of sympathetic vasomotor tone in animal models of central baroreflex failure.[20–22] As a crucial first step to clinical application, we tested its feasibility and efficacy in a clinical model of orthostatic hypotension. A percutaneous epidural catheter approach was established for the monitoring of spinal function during surgery and for pain management,[28] and the lower thoracic level was selected for spinal cord stimulation based on earlier reports that the abdominal splanchnic vascular bed is a major effector mechanism for arterial baroreflex in animals[23,24] and humans.[25] Although the percutaneous epidural approach is less invasive than implantation surgery, spinal cord stimulation excites motor and sensory nerves[12,22,28] in addition to sympathetic vasomotor efferents. Therefore, administration of sufficient doses of muscle relaxants and analgesics was required during experimental protocols. Under these conditions, the dynamic response of AP to STM was easily characterized by the white noise system identification method. Furthermore, the quantitatively estimated results of transfer function analysis (Figure 2B) enabled simulation of the effects of feedback correction factors[27] on performance of the BBS. As demonstrated in Figure 3, the simulation results suggested that the specific combination of feedback correction factors could optimize the performance of the BBS. On the basis of these results, the feedback correction factors were determined to allow the BBS to quickly stabilize AP against the external disturbances.

Efficacy of BBS

The present study utilized a tourniquet-related model of hypotension[29–31] during general anesthesia[32,33] to approximate orthostatic hypotension due to central baroreflex failure. Except for the change in peripheral vascular resistance, the hemodynamic changes after tourniquet deflation are similar to those achieved after upright tilt-

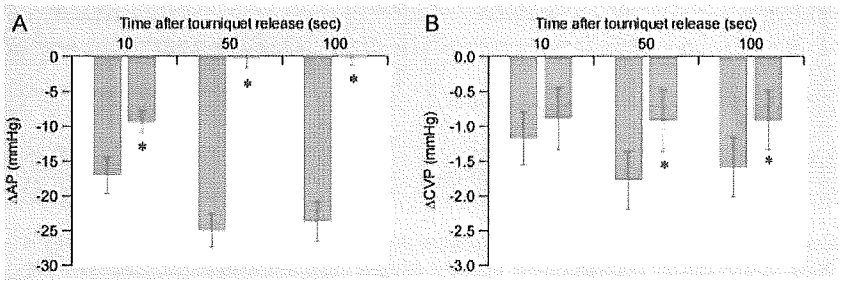

Figure 5. Bar graphs showing changes in AP (A) and CVP (B) at 10, 50, and 100 seconds after tourniquet release. Implementation of the BBS (red column) significantly attenuated tourniquet-related falls (blue column) in AP and CVP. Data are expressed as mean±SD for 21 patients. *Overall $P<0.05$.

ing.[29,31] For example, tourniquet release results in a rapid increase in venous pooling in the affected limb with a subsequent decrease in venous return and cardiac output. Under general anesthesia with volatile gases such as sevoflurane,[32,33] arterial baroreflex function is inhibited, and the hemodynamic disturbance produced by the tourniquet inevitably results in abrupt hypotension. In rare instances, tourniquet deflation can also trigger fatal circulatory collapse.[29]

Despite the fact that the BBS was implemented with fixed values of feedback correction factors for all patients, the BBS successfully stabilized AP against the hemodynamic challenge induced by sudden tourniquet release (Figure 4). These data indicate that the BBS may compensate for some individual differences in the dynamic response of AP to STM.

Finally, the CVP response to STM (Figure 4) in the present study suggests that the BBS attenuated a decrease in venous return. Previous studies have demonstrated that the baroreflex-mediated vasoconstriction in the splanchnic vascular bed is a major mechanism for recruitment of venous return during head-up tilting.[23,25] Therefore, the BBS may functionally mimic the baroreflex control of venous return and control of AP.

Study Limitations

This study possessed several limitations. First, based on the previous results[20–22] obtained from animal studies, the stimulation electrodes were placed in the epidural space at the level of the lower thoracic cord; however, further study to determine the optimal site of electrode placement would be of benefit. Second, it is unclear whether or not the feedback controller designed in the present study is universally applicable to other cases. Although preset parameters for feedback correction were used in the present study, other approaches based on a robust control theory could yield a better result. Finally, the epidural catheter method for sympathetic nerve stimulation is associated with significant pain and discomfort. Thus, practical use of the BBS requires an appropriate method for stimulating only efferent sympathetic nerves.

Clinical Implications

The present study confirmed the efficacy of the BBS in a clinical setting and suggests that the BBS has tremendous potential as a new therapeutic modality for treatment of severe orthostatic intolerance in patients with various syndromes of central baroreflex failure, including Shy-Drager syndrome, baroreceptor deafferentation, and traumatic spinal cord injuries.

Acknowledgments

This study was supported by a Health and Labor Sciences research grant (H14-NANO-002, H16-NANO-005, H15-KOKORO-019) from the Ministry of Health, Labor, and Welfare of Japan and by a grant-in-aid for scientific research (15300165) from the Ministry of Education, Science, Sports, and Culture of Japan.

Disclosures

None.

References

1. Guyton AC, Coleman TG, Granger HJ. Circulation: overall regulation. *Ann Rev Physiol.* 1972;34:13–46.
2. Robertson D. Diagnosis and management of baroreflex failure. *Primary Cardiol.* 1995;21:37–40.
3. Sunagawa K, Sato T, Kawada T. Integrative sympathetic baroreflex regulation of arterial pressure. *Ann N Y Acad Sci.* 2001;940:314–323.
4. Ketch T, Biaggioni I, Robertson R, Robertson D. Four faces of baroreflex failure: hypertensive crisis, volatile hypertension, orthostatic tachycardia, and malignant vagotonia. *Circulation.* 2002;105:2518–2523.
5. Sato T, Kawada T, Inagaki M, Shishido T, Takaki H, Sugimachi M, Sunagawa K. New analytical framework for understanding the sympathetic baroreflex control of arterial pressure. *Am J Physiol Heart Circ Physiol.* 1999;276:H2251–H2261.
6. Shy M, Drager GA. A neurological syndrome associated with orthostatic hypotension: a clinico-pathologic study. *Arch Neurol.* 1960;3:511–527.
7. The Consensus Committee of the American Autonomic Society and the American Academy of Neurology. Consensus statement on the definition of orthostatic hypotension, pure autonomic failure, and multiple system atrophy. *Neurology.* 1996;46:1470.
8. Schatz IJ. Farewell to the "Shy-Drager syndrome." *Ann Intern Med.* 1996;125:74–75.
9. Goldstein DS, Holmes C, Cannon RO III, Eisenhofer G, Kopin IJ. Sympathetic cardioneuropathy in dysautonomias. *N Engl J Med.* 1997;336:696–702.
10. Onrot J, Wiley RG, Fogo A, Biaggioni I, Robertson D, Hollister AS. Neck tumour with syncope due to paroxysmal sympathetic withdrawal. *J Neurol Neurosurg Psychiatry.* 1987;50:1063–1066.
11. Lee HT, Brown J, Fee WE Jr. Baroreflex dysfunction after nasopharyngectomy and bilateral carotid isolation. *Arch Otolaryngol Head Neck Surg.* 1997;123:434–437.
12. Frankel HL, Mathias CJ. Severe hypertension in patients with high spinal cord lesions undergoing electro-ejaculation: management with prostaglandin E_2. *Paraplegia.* 1980;18:293–299.
13. Matthews JM, Wheeler GD, Burnham RS, Malone LA, Steadward RD. The effects of surface anaesthesia on the autonomic dysreflexia response during functional electrical stimulation. *Spinal Cord.* 1997;35:647–651.
14. Wilcox CS, Puritz R, Lightman SL, Bannister R, Aminoff MJ. Plasma volume regulation in patients with progressive autonomic failure during changes in salt intake or posture. *J Lab Clin Med.* 1984;104:331–339.
15. Jordan J, Shannon JR, Diedrich A, Black B, Robertson D, Biaggioni I. Water potentiates the pressor effect of ephedra alkaloids. *Circulation.* 2004;109:1823–1825.
16. Kristinsson A. Programmed atrial pacing for orthostatic hypotension. *Acta Med Scand.* 1983;214:79–83.
17. Bannister R, da Costa DF, Hendry WG, Jacobs J, Mathias CJ. Atrial demand pacing to protect against vagal overactivity in sympathetic autonomic neuropathy. *Brain.* 1986;109:345–356.
18. Kachi T, Iwase S, Mano T, Saito M, Kunimoto M, Sobue I. Effect of L-threo-3,4-dihydroxyphenylserine on muscle sympathetic nerve activities in Shy-Drager syndrome. *Neurology.* 1988;38:1091–1094.
19. Obara A, Yamashita H, Onodera S, Yahara O, Honda H, Hasebe N. Effect of xamoterol in Shy-Drager syndrome. *Circulation.* 1992;85:606–611.
20. Sato T, Kawada T, Shishido T, Sugimachi M, Alexander J Jr, Sunagawa K. Novel therapeutic strategy against central baroreflex failure: a bionic baroreflex system. *Circulation.* 1999;100:299–304.
21. Sato T, Kawada T, Sugimachi M, Sunagawa K. Bionic technology revitalizes native baroreflex function in rats with baroreflex failure. *Circulation.* 2002;106:730–734.
22. Yanagiya Y, Sato T, Kawada T, Inagaki M, Tatewaki T, Zheng C, Kamiya A, Takaki H, Sugimachi M, Sunagawa K. Bionic epidural stimulation restores arterial pressure regulation during orthostasis. *J Appl Physiol.* 2004;97:984–990.
23. Hainsworth R, Karim F. Responses of abdominal vascular capacitance in the anaesthetized dog to changes in carotid sinus pressure. *J Physiol Lond.* 1976;262:659–677.

24. Carneiro JJ, Donald DE. Blood reservoir function of dog spleen, liver, and intestine. *Am J Physiol Heart Circ Physiol.* 1977;232:H67–H72.
25. Minson CT, Wladkowski SL, Pawelczyk JA, Kenney WL. Age, splanchnic vasoconstriction, and heat stress during tilting. *Am J Physiol Regul Integr Comp Physiol.* 1999;276:R203–R212.
26. Marmarelis PZ, Marmarelis VZ. *Analysis of Physiological Systems: The White-Noise Approach.* New York, NY: Plenum; 1978.
27. Kawada T, Sunagawa G, Takaki H, Shishido T, Miyano H, Miyashita H, Sato T, Sugimachi M, Sunagawa K. Development of a servo-controller of heart rate using treadmill. *Jpn Circ J.* 1999;63:945–950.
28. Shimoji K, Hokari T, Kano T, Tomita M, Kimura R, Watanabe S, Endoh H, Fukuda S, Fujiwara N, Aida S. Management of intractable pain with percutaneous epidural spinal cord stimulation: differences in pain-relieving effects among diseases and sites of pain. *Anesth Analg.* 1993;77:110–116.
29. Kahn RL, Marino V, Urquhart B, Sharrock NE. Hemodynamic changes associated with tourniquet use under epidural anesthesia for total knee arthroplasty. *Reg Anesth.* 1992;17:228–232.
30. Feldman DL, Wigod M, Barwick W, Levin LS. Tourniquet-related hypotension in venous stasis ulcer excision. *Ann Plast Surg.* 1993;30:556–559.
31. Sander-Jensen K, Mehlsen J, Secher NH, Bach FW, Bie P, Giese J, Schwartz TW, Trap-Jensen J, Warberg J. Progressive central hypovolaemia in man–resulting in a vasovagal syncope? Haemodynamic and endocrine variables during venous tourniquets of the thighs. *Clin Physiol.* 1987;7:231–242.
32. Tanaka M, Nishikawa T. Arterial baroreflex function in humans anaesthetized with sevoflurane. *Br J Anaesth.* 1999;82:350–354.
33. Keyl C, Schneider A, Hobbhahn J, Bernardi L. Sinusoidal neck suction for evaluation of baroreflex sensitivity during desflurane and sevoflurane anesthesia. *Anesth Analg.* 2002;95:1629–1636.

CLINICAL PERSPECTIVE

Central baroreflex failure due to Shy-Drager syndrome, baroreceptor deafferentation, and traumatic spinal cord injuries results in severe orthostatic hypotension. However, most commonly used interventions, such as salt loading, cardiac pacing, and pharmacological approaches, can neither restore nor reproduce the functioning of a native vasomotor center. Here, we proposed a novel therapeutic strategy against central baroreflex failure and developed a bionic baroreflex system (BBS). The BBS consisted of a pressure sensor, computer, electrical stimulator, and epidural catheter with sympathetic nerve stimulation electrodes. While automatically calculating the frequency of a pulse train in response to a change in arterial pressure, the computer drove the stimulator at the appropriate frequency to stabilize arterial pressure against an external disturbance. According to a parametric negative-feedback control theory, we designed an algorithm of the computer functioning as an artificial vasomotor center. The efficacy of the BBS was tested in a clinical model of orthostatic hypotension during knee joint surgery. Without the implementation of the BBS, a sudden deflation of a thigh tourniquet resulted in rapid progressive hypotension. By contrast, during real-time execution of the BBS, arterial pressure was quickly restored to the baseline level before tourniquet release. These results suggest the technical feasibility of functional restoration of arterial baroreflex with the BBS.

REGULAR PAPER

J. Physiol. Sci. Vol. 56, No. 1; Feb. 2006; pp. 95–101
Online Feb. 25, 2006; **DOI: 10.2170/physiolsci.RP002305**

Nitric Oxide Stimulates Vascular Endothelial Growth Factor Production in Cardiomyocytes Involved in Angiogenesis

Masanori KUWABARA[1,2], Yoshihiko KAKINUMA[1], Motonori ANDO[1], Rajesh G. KATARE[1], Fumiyasu YAMASAKI[3], Yoshinori DOI[2], and Takayuki SATO[1]

[1]Department of Cardiovascular Control, Kochi Medical School, Nankoku, Japan; [2]Department of Medicine and Geriatrics, Kochi Medical School, Nankoku, Japan; and [3]Department of Clinical Laboratory, Kochi Medical School, Nankoku, Japan

Abstract: Background: Hypoxia-inducible factor (HIF)-1α regulates the transcription of lines of genes, including vascular endothelial growth factor (VEGF), a major gene responsible for angiogenesis. Several recent studies have demonstrated that a nonhypoxic pathway via nitric oxide (NO) is involved in the activation of HIF-1α. However, there is no direct evidence demonstrating the release of angiogenic factors by cardiomyocytes through the nonhypoxic induction pathway of HIF-1α in the heart. Therefore we assessed the effects of an NO donor, S-Nitroso-N-acetylpenicillamine (SNAP) on the induction of VEGF via HIF-1α under normoxia, using primary cultured rat cardiomyocytes (PRCMs). Methods and Results: PRCMs treated with acetylcholine (ACh) or SNAP exhibited a significant production of NO. SNAP activated the induction of HIF-1α protein expression in PRCMs during normoxia. Phosphatidylinositol 3-kinase (PI3K)–dependent Akt phosphorylation was induced by SNAP and was completely blocked by wortmannin, a PI3K inhibitor, and N^G-nitro-L-arginine methyl ester (L-NAME), a NO synthase inhibitor. The SNAP treatment also increased VEGF protein expression in PRCMs. Furthermore, conditioned medium derived from SNAP-treated cardiomyocytes phosphorylated the VEGF type–2 receptor (Flk-1) of human umbilical vein endothelial cells (a fourfold increase compared to the control group, $p < 0.001$, $n = 5$) and accelerated angiogenesis. Conclusion: Our results suggest that cardiomyocytes produce VEGF through a nonhypoxic HIF-1α induction pathway activated by NO, resulting in angiogenesis.

Key words: vascular endothelial growth factor, angiogenesis, cardiomyocyte, Flk-1, nitric oxide.

The prognosis of patients with chronic heart failure remains poor because of progressive remodeling of the heart and lethal arrhythmia [1]. It has recently been reported that vagal nerve stimulation therapy markedly improved long-term survival in an animal model of chronic heart failure after myocardial infarction [2] and that acetylcholine (ACh) has a direct cardioprotective effect through the PI3K-Akt-hypoxia-inducible factor (HIF)-1α pathway [3, 4]. Nitric oxide (NO) is supposed to be one of the signaling molecules induced by ACh; however, it remains to be clarified whether NO is involved in angiogenesis through the nonhypoxic induction pathway of HIF-1α and vascular endothelial growth factor (VEGF), and is thereby related to the cardioprotective effects of ACh or vagal nerve stimulation.

VEGF is a key angiogenic factor and major target of HIF-1α, which is produced by ischemic tissue and growing tumors [5–7]. Factors including VEGF secreted by noncardiomyocytes are known to possess significant paracrine effects on cardiomyocytes; however, the importance of such cardiomyocyte-derived factors as paracrine or autocrine effectors on angiogenesis in the heart remains to be elucidated. The HIF-1α protein level is usually regulated by the oxygen concentration. During hypoxia, HIF-1α protein is stabilized by escaping from degradation through von Hippel-Lindau tumor-suppressor protein (VHL) [8, 9]. Furthermore, the PI3K-Akt signaling pathway, which is known for the antiapoptotic functions [10, 11], is demonstrated to be involved in HIF-1α induction [12]. Recently it has been revealed that besides hypoxia, certain cytokines, growth factors, and NO increase the HIF-1α protein level even under the normoxic conditions in some specific cells [13–15]. To our knowledge, however, the involvement of NO in this signaling pathway in cardiomyocytes under normoxic conditions remains to be elucidated. Moreover, it is also unclear whether NO is involved in angiogenesis in the heart, though NO is associated with many aspects of cellular biology involved in cell signaling, vasodilatory tone, and cell growth [16].

With this background, we speculated the nonhypoxic induction of HIF-1α in the cardiomyocytes through NO-mediated pathway and that NO plays another role in producing an angiogenic factor through the pathway. To prove this hypothesis, we assessed the effect of a NO do-

Received on Dec 2, 2005; accepted on Feb 5, 2006; released online on Feb 25, 2006; DOI: 10.2170/physiolsci.RP002305
Correspondence should be addressed to: Yoshihiko Kakinuma, Department of Cardiovascular Control, Kochi Medical School, Nankoku, Kochi, 783-8505 Japan. Fax: +81-88-880-2310, Tel: +81-88-880-2587, E-mail: kakinuma@med.kochi-u.ac.jp